AFRL-OSR-VA-TR-2014-0107

ACTIVE STRUCTURAL FIBERS FOR MULTIFUNCTIONAL COMPOSITE MATERIALS

Henry Sodano
ARIZONA STATE UNIVERSITY

05/06/2014
Final Report

Air Force Research Laboratory
AF Office Of Scientific Research (AFOSR)/ RSA
Arlington, Virginia 22203
Air Force Materiel Command

REPORT DOCUMENTATION PAGE

Form Approved
OMB No. 0704-0188

1. REPORT DATE *(DD-MM-YYYY)*	2. REPORT TYPE	3. DATES COVERED *(From - To)*
Oct. 31, 2011	Final Report	

4. TITLE AND SUBTITLE
Active Structural Fibers for Multifunctional Composite Materials

5a. CONTRACT NUMBER
FA9550-08-1-0383

5b. GRANT NUMBER

5c. PROGRAM ELEMENT NUMBER

6. AUTHOR(S)
Henry A. Sodano

5d. PROJECT NUMBER

5e. TASK NUMBER

5f. WORK UNIT NUMBER

7. PERFORMING ORGANIZATION NAME(S) AND ADDRESS(ES)
Arizona State Univeristy
501 East Tyler Mall, MC 6106
Tempe, AZ 85287-6106

8. PERFORMING ORGANIZATION REPORT NUMBER

9. SPONSORING / MONITORING AGENCY NAME(S) AND ADDRESS(ES)
Mechanics of Multifunctional Materials & Microsystems
Air Force Office of Scientific Research
875 N. Randolph Street, AFOSR/NA, Suite 325, Room 3112
Arlington, VA 22203

10. SPONSOR/MONITOR'S ACRONYM(S)

11. SPONSOR/MONITOR'S REPORT NUMBER(S)

12. DISTRIBUTION / AVAILABILITY STATEMENT
Distribution Statement A

13. SUPPLEMENTARY NOTES

14. ABSTRACT

The objective of this proposed research program is to investigate the development of a multifunctional material system through the deposition of a piezoelectric film on the surface of a carbon based reinforcing fiber. Piezoelectric materials have a crystalline structure in which the application of an electrical potential generates mechanical strain and vise versa, an applied stress will result in the generation of an electric charge. When piezoelectric materials are used for sensing mechanical vibration the voltage output can be dissipated through a shunt circuit to induce damping in the structure or can be stored and used to power other electronics. Each of these separate functions have significant benefits for DoD applications and together will proved a single material with selective functionality dependent on its use. This program will scale the active fiber from a SiC core (140μm) to a carbon fiber core (5μm) and perform nanoscale testing to characterize the electromechanical properties of the active fiber. Furthermore, the functionality of this new material for constructing multifunctional materials will be demonstrated.

15. SUBJECT TERMS

16. SECURITY CLASSIFICATION OF:			17. LIMITATION OF ABSTRACT	18. NUMBER OF PAGES	19a. NAME OF RESPONSIBLE PERSON
a. REPORT	b. ABSTRACT	c. THIS PAGE			19b. TELEPHONE NUMBER *(include area code)*
					Henry Sodano 352-273-2663

Standard Form 298 (Rev. 8-98)
Prescribed by ANSI Std. Z39.18

To: technicalreports@afosr.af.mil
Subject: Annual Progress Statement to Dr. Les Lee

Contract/Grant Title: Active Structural Fibers for Multifunctional Composite Materials

Contract/Grant #: FA9550-08-1-0383

During the current reporting period the development of a multifunctional fiber has been investigated. The design utilizes the fiber as both the electrode and load bearing element such that when embedded into a composite both strength and electromechanical responsiveness can be capitalized upon. Theoretical and finite element models of the fiber and a lamina incorporating it were developed and shown to have excellent agreement with each other. Synthesis techniques for the active structural fiber were developed using electrophoretic deposition and characterized using a novel AFM technique. The results of this testing have validated the accuracy of the model and demonstrated that structural composites could be developed with electromechanical coupling nearly 70% of the active constituent's bulk properties. Additionally, the use of the fiber for a structural capacitor has been investigated and the results showed performance from a load-bearing member comparable to commercial capacitors. Lastly, a cathodic electrolytic deposition process has been investigated for the coating of carbon fibers with a PZT shell. The results have demonstrated the ability to use the process to coat fibers with a thin shell of PZT. The results thus far have demonstrated the feasibility of the multifunctional composite and the potential to create responsive structures.

Archival publications (published) during reporting period:

1. Lin, Y., Zhi, Z. and Sodano, 2012, "Barium Titanate and Barium Strontium Titanate Coated Carbon Fibers for Multifunctional Structural Capacitors," *Journal of Composite Materials*, In Review.

2. Zhou, Z., Lin, Y. and Sodano, H.A., Synthesis and Characterization of Textured BaTiO3 Thin Films, 36th International Conference and Expo on Advanced Ceramics and Composites, January 22 – 27, 2012, Daytona Beach, FL.

3. Sodano, H.A., 2011, "Nanowire Interfaces for Simultaneously Increased Strength and Functionality, Composites at Lake Louise Conference, October 30th – November 4th, Alberta, Canada (Invited Speaker).

4. Sodano, H.A., 2011, "Multifunctional Materials and Nanocomposites for Energy Storage," Nanotechnology for Defense Conference (NT4D), October 24 – 27, Bellevue, WA (Invited Speaker).

5. Sodano, H.A., 2011, "Multifunctional Solutions for Piezoelectric Energy Harvesting," International Symposium on Green Manufacturing and Applications (ISGMA 2011), October 6 – 7, Seoul National University, Seoul, Korea (Keynote Speaker).

6. Lin, Y. and Sodano, H.A., 2010, "Enhanced piezoelectric properties of lead zirconate titanate sol-gel derived ceramics using single crystal $PbZr_{0.52}Ti_{0.48}O_3$ cubes," *Journal of Applied Physics*, 108, 064108.

7. Lin, Y., Zhou, Z. and Sodano, H.A., 2011, "Multifunctional Structural Capacitors Consisting of Barium Titanate and Barium Strontium Titanate Coated Carbon Fibers, 18th International Conference on Composite Materials, August 21-26, Jeju Island, South Korea.

8. Lin, Y. and Sodano H.A. 2011 "Multifunctional Structural Capacitors Consisting of Barium Strontium Titanate Coated SiC Fibers," Electronic Materials and Applications 2011, Jan. 19th–21st Orlando, FL (Invited).

9. Lin, Y., Shaffer, J.W. and Sodano, H.A., 2010, Electrolytic Deposition of PZT on Carbon Fibers for Multifunctional Composites, *Smart Materials and Structures*, **19**: 124004 (Invited paper).

10. Lin, Y. and Sodano, H.A., 2010, "Double Inclusion Model for Multiphase Piezoelectric Composites," *Smart Materials and Structures*, **19**: 035003.

11. Lin, Y. and Sodano H.A., 2009, "Characterization of Multifunctional Structural Capacitors for Embedded Energy Storage," *Journal of Applied Physics*, **106**: 114108.

12. Lin, Y. and Sodano, H.A., 2009, "Electromechanical Characterization of a Multifunctional Active Structural Fiber Lamina," *Composites Science and Technology*, **69**: 1825–1830.

13. Lin, Y. and Sodano, H.A., 2009, "Fabrication and Electromechanical Characterization of a Piezoelectric Structural Fiber for Multifunctional Composites," *Advanced Functional Materials*, **19**: 1-7.

14. Lin, Y. and Sodano, H.A., 2008, "Concept and Model of a Piezoelectric Structural Fiber for Multifunctional Composites," *Composites Science and Technology*, **68** (7-8):1911-1918.

15. Lin, Y. and Sodano, H.A., 2009, "Double Inclusion Model for Multiphase Piezoelectric Composites," *Smart Materials and Structures*, In Review.

16. Shaffer, J.W., Lin, Y. and Sodano, H.A., 2009, Electrolytic Deposition of PZT on Carbon Fibers for Multifunctional Composites, Proceeding of the 15th International Conference on Adaptive Structures and Technologies (ICAST), October 20th – 22nd, Hong Kong, China.

17. Lin, Y. and Sodano H.A., 2009, "Characterization of Multifunctional Structural Capacitors for Embedded Energy Storage," ASME's 2nd Annual Conference on Smart Materials, Adaptive Structures and Intelligent Systems, September 21st-23rd Oxnard, CA.

18. Lin, Y. and Sodano, H.A., 2009, "Double Inclusion Model for Multifunctional Piezoelectric Composites," Proceedings of the 50th AIAA/ASME/ASCE/AHS/ASC Structures, Structural Dynamics and Materials Conference (SDM), May 4-7th, Palm Springs, CA.

19. Lin, Y. and Sodano, H.A., 2009, Electromechanical Characterization of Single Active Structural Fiber for Multifunctional Composites, Proceeding of the 15th International Conference on Adaptive Structures and Technologies (ICAST), October 20th – 22nd, Hong Kong, China.

20. Lin, Y. and Sodano, H.A., 2009, "Electromechanical Characterization of a Single Fiber Lamina for Multifunctional Composites," SPIE's 16th annual International Symposium on

Smart Structures and Materials, March 8th-12th, San Diego, CA.

21. Lin, Y. and Sodano, H.A., 2008, "Fabrication and Electromechanical Characterization of a Piezoelectric Structural Fiber for Multifunctional Composites," 2008 SAMPE Fall Technical Conference, Sept. 8-11th, Memphis, TN. ***(Awarded Best Paper)***

22. Lin, Y. and Sodano, H.A., 2008, "Concept and Model of a Piezoelectric Structural Fiber for Multifunctional Composites," SPIE's 15th annual International Symposium on Smart Structures and Materials, March 9th-13th, San Diego, CA.

Changes in research objectives, if any: None

Change in AFOSR program manager, if any: None

Extensions granted or milestones slipped, if any: None

Include any new discoveries, inventions, or patent disclosures during this reporting period (if none, report none): None

ACTIVE STRUCTURAL FIBERS FOR MULTIFUNCTIONAL COMPOSITES

Henry A. Sodano
Department of Mechanical and Aerospace Engineering
Arizona State University
501 East Tyler Mall, ECG 346
Tempe, AZ 85287-6106
Office: 480-965-4317 Fax: 480-965-1384
Henry.sodano@asu.edu

1.0 Introduction

Multifunctional materials are designed to accomplish multiple tasks, one of which is often load bearing, through the use of a single material or structure. Piezoelectric materials can provide a structure with a variety of functionalities such as sensing, actuation, self-monitoring, damping, etc. however piezoelectric materials are generally not suitable for load bearing applications. In the monolithic form, piezoelectric materials are vulnerable to accidental breakage during handling and bonding procedures, have an extremely limited ability to conform to curved surfaces and lead to large add on mass due to the typically lead-based ceramic. To resolve the inadequacies of monolithic piezoceramic materials, researchers have developed composite piezoelectric devices consisting of an active piezoceramic fiber embedded in a polymer matrix. The polymer matrix acts to improve the flexibility of the actuator and protects the fragile fibers.

The use of piezoelectric composite actuators has traditionally been motivated for use in structural applications. Sodano et al. [1, 2] showed their potential for dynamic testing and control of ultra-lightweight inflatable space structures. However, the materials are often difficult to embed because the electrodes are separate from the fiber and the required interconnects can compromise the composites strength. Additionally, the tensile modulus of the piezoceramic fiber used in PFCs is generally 4~5 times lower than that of traditional composite reinforcements and thus the addition of these active fillers provide little strength to the composite structure. For this reason, PFCs have typically been applied as surface-bonded patches to perform sensing and actuation. The limitations encountered by PFCs can be avoided through the use of embedded electrodes. The majority of work in this area has focused on the use of a metal core electrode. Sebald [3] used extrusion methods to produce fibers with a platinum core surrounded by a PNN-PZT/polymer binder which was fired to leave a platinum/PNN-PZT core shell fiber. Experimental results showed the electromechanical coupling of the fiber to have a d_{31} piezoelectric coupling as high as -112pC/N (45.5 % of that of the bulk material). Takagi et al. [4] embedded a PZT coated platinum fiber in a carbon fiber reinforced plastic (CFRP) to form a "smart board" for vibration suppression. More recently Sato et al. [5] applied a hydrothermal method to grow PZT coating onto nickel titanium wires.

While the embedded metal electrode can provide the advantage of integrated electrical interconnects, the ductility of the core can lead to surface cracking under strain. Additionally, the plastic nature and high coefficient of thermal expansion of metallic materials can lead to high residual stresses in the ceramic coating. Therefore our research effort under this AFOSR program is investigating the use of carbon based fibers to provide an electrical interconnect and structural reinforcement to create a multifunctional active structural fiber. The configuration of the multifunctional fiber is shown in Figure 1. Our research program has currently developed theoretical models for the electromechanical coupling of the Active Structural Fiber (ASF), validated this model through finite element testing, developed laboratory manufacturing process for the fabrication of the fiber and performed a validation of the longitudinal displacement of the fiber and a lamina. Additionally, experiments have been performed

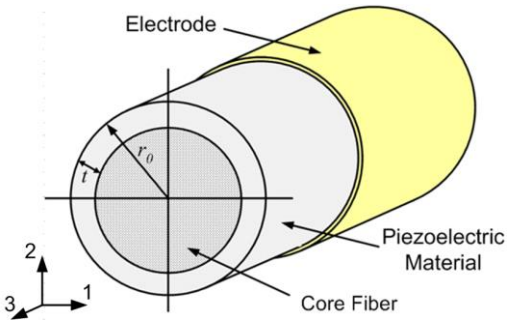

Figure 1: Schematic showing the cross-section of the novel multifunctional fiber.

2.0 Micromechanics Model of Longitudinal Electromechanical Response

Our efforts under this grant have developed two models to predict the properties of the ASF. The first formulation is a 1-dimensional model that allows for the prediction of the electromechanical coupling coefficient in the fiber axis while the second is based on the double inclusion micromechanics model and allows the prediction of the entire set of electroelastic constitutive properties.

2.1 One-Dimensional Model of the Electromechanical Coupling

The electric field applied to the ASF occurs in the radial direction of the fiber between the conductive core fiber and the electrode applied to the outer surface of the piezoceramic shell. Because the inner electrode has a smaller surface area than the outer electrode, the electric field will vary nonlinearly through the thickness of the piezoceramic. This nonlinear field variation must be accounted for such that the breakdown voltage at the inner wall of the fiber is not reached. From Gauss' Law, the thin wall electric field approximation along the radial direction of the active fiber can be expressed as

$$E(r) = \frac{-V}{r\ln(1-\alpha)} \tag{1}$$

where V is the voltage applied across the fiber thickness, r is the radial position, and α is the aspect ratio of the piezoelectric portion of the fiber, equal to t/r_0, where t is the thickness of the piezoelectric coating and r_0 is the total radius of the fiber. Using the thin wall approximation, the longitudinal piezoelectric stress of the piezoelectric shell can be expressed as

$$\sigma(r) = Y^p \varepsilon(r) = Y^p d_{31} E(r) \tag{2}$$

where Y^p is the longitudinal modulus of elasticity of the piezoelectric shell, σ is the piezoelectric shell longitudinal stress, ε is the piezoelectric shell longitudinal strain, and d_{31} is the piezoelectric coupling. The subscript *-31* is used to denote that the electric field is applied in the -3 direction while the strain output in is the -1 direction (see Figure 1). The total piezoelectric force is then determined by integrating the stress over the cross-section area of the piezoelectric shell, defined as

$$F = \int_0^{2\pi}\int_{r_0-t}^{r_0} Y^p d_{31} E(r) r\,dr\,d\theta = \frac{-2\pi d_{31} Y^p V t}{\ln(1-t/r_0)}. \tag{3}$$

The free strain resulting from the total piezoelectric force can then be derived using Equation 3 and Hook's law and realizing the free strain can be expressed as the product of thin wall electric field $E_{tw}=V/t$ and the effective piezoelectric coupling of the ASF $d^f_{31,eff}$, defined as

$$\varepsilon = \frac{\sigma}{Y^p} = \frac{F}{AY^p} = \frac{-2\pi d_{31} Y^p V t}{\pi\left[r_o^2 - \left(r_o + t^2\right)\right] Y^P \ln(1-t/r_o)} = \left(\frac{-d_{31}}{\ln(1-\alpha)(1/\alpha - 0.5)}\right) E_{tw} = d^f_{31,eff} E_{tw} \tag{4}$$

where $E_{tw}=V/t$ is the electric field derived by thin wall approximation, A is the cross-sectional area of the piezoelectric shell, F is the piezoelectric force, d_{31} is the coupling coefficient and $d^f_{31,eff}$ is the effective coupling of the piezoelectric shell.

The coupling for the piezoelectric shell must be then combined with the core fiber to determine the effective piezoelectric coupling of the piezoelectric structural fiber. The longitudinal elastic modulus of the active fiber containing a core fiber can be defined using the rule of mixtures and written as

$$Y^{multi} = Y^{p}v^{p} + Y^{f}(1-v^{p}) \tag{5}$$

where Y is the longitudinal modulus of elasticity, v is the volume fraction and the superscripts f, p and *multi* represent the core fiber, piezoelectric, and complete multifunctional piezoelectric structural fiber, respectively. According to equation (4), the piezoelectric force generated by the piezoelectric shell can be expressed as

$$F = A\varepsilon Y^{p} = \frac{-E_{tw}d_{31}}{\left(r_o/t-0.5\right)\ln\left(1-t/r_0\right)}AY^{p} = E_{tw}d_{31,eff}^{f}AY^{p}\ . \tag{6}$$

Then using the Hook's law the total strain of the ASF caused by the piezoelectric force is

$$\varepsilon^{multi} = \frac{\sigma^{multi}}{Y^{multi}} = \frac{\overline{F}}{\overline{A/v^{p}}}\frac{}{Y^{multi}} = \frac{d_{31,eff}^{f}Y^{p}v^{p}E_{tw}}{Y^{multi}} = d_{31}^{multi}E_{tw}. \tag{7}$$

The electromechanical coupling of a piezoelectric structural fiber with a piezoelectric coating can therefore be defined as

$$d_{31}^{multi} = \frac{d_{31,eff}Y^{p}v^{p}}{\left(Y^{p}-Y^{f}\right)v^{p}+Y^{f}} \tag{8}$$

where Y^p and Y^f are the elastic modulus of the piezoelectric material and fiber, respectively, v^p is the volume fraction of piezoelectric material, d_{31} is the piezoelectric coupling coefficient and $d_{31,eff}$ is the effective coupling of the piezoelectric shell as defined from equation (4).

The piezoelectric coupling term in Equation (8) predicts the response of a single active fiber, however, in order to determine the coupling when multiple active fibers are embedded in a polymer matrix, the rule of mixtures can be applied again a second time by taking the piezoelectric shell to be an interphase layer. Similar in derivation as Equation (8), the resulting coupling can then be written as

$$d_{31}^{lam} = \frac{d_{31,eff}Y^{p}v^{p}}{\left(Y^{p}-Y^{m}\right)v^{p}+\left(Y^{f}-Y^{m}\right)v^{f}+Y^{m}} \tag{9}$$

where Y^m is the modulus of elasticity of the matrix material, and v^f is the volume fraction of the core fiber. The equations defining the electromechanical coupling of the piezoelectric structural fiber can now be applied to study the effect the fiber geometry has on the response of the fiber. The free strain equation can then be used with FEM analysis or experiments to validate the theoretically predicted electromechanical coupling along the fiber length.

2.2 Double Inclusion Model

When modeling composites where the inclusions consist of layered multiphase materials the double inclusion model proposed by Hori and Nemat-Nasser [6] has provided accurate results for the average stress and strain in a double inclusion (an inclusion embedded in a second inclusion) containing an eigenstrain distribution. The current literature has shown the double inclusion model to be a powerful method for the prediction of the effective elastic properties of composites with multiphase and multilayered inclusions. However, the model's capability to estimate the electroelastic properties of the multiphase piezoelectric composites is yet unknown and the model's current form is not applicable to active materials. The modeling approach developed here provides the framework required to extend the double inclusion approach for the prediction of the electroelastic properties of multi-phase piezoelectric composites. The results provide a new model to predict the effective electroelastic properties of three or more phase multifunctional composites.

Considering a transversely isotropic piezoelectric material, the linear constitutive equations used to describe the coupled interaction between the electrical and mechanical variables can be expressed as

$$\begin{bmatrix} \sigma_{ij} \\ D_i \end{bmatrix} = \begin{bmatrix} C_{ijmn} & -e_{nij} \\ e_{imn} & \kappa_{in} \end{bmatrix} \begin{bmatrix} \varepsilon_{mn} \\ E_n \end{bmatrix} \tag{10}$$

where σ_{ij}, ε_{mn}, E_n and D_i are the stress, strain, electric field and electric displacement tensors, respectively, and the C_{ijmn}, e_{nij} and κ_{in} are elastic (at a constant electric field), piezoelectric field-stress (in a constant strain or electric field) and dielectric (at a constant strain) tensors, respectively.

For an inhomogeous composite with piezoelectric inclusions, it is convenient to combine the mechanical and electrical variables such that the two equations can be expressed in a single constitutive equation [7]. This notation is identical to conventional indicial notation with the exception that lower case subscripts are in the rage of 1-3, while the capitalized subscripts are in the range of 1-4 and repeated capitalized subscripts summed over 1-4. Assuming perfect bonding between all the phases in the composites, the general expression of the volume averaged piezoelectric fields of the multiphase active composites can be expressed as [8]

$$\overline{\Sigma} = \sum_{r=1}^{N} c_r \overline{\Sigma}_r \tag{11}$$

$$\overline{Z} = \sum_{r=1}^{N} c_r \overline{Z}_r \tag{12}$$

where c is the volume fraction, the subscript r represents r^{th} phase of the composites, with 1 representing the matrix phase, the bars denote the volume average of the quantities. Considering the piezoelectric composites subjected to homogeneous elastic strain and electric potential boundary conditions, Z^0, the volume averaged strain and electric field $\overline{Z}$ equals to Z^0 [9]. Therefore, equation (6) can be represented as

$$\overline{\Sigma} = E\overline{Z} \tag{13}$$

noting that the volume averaged strain and electric field in r^{th} phase is expressed as

$$\overline{Z}_r = A_r \overline{Z} \tag{14}$$

where A_r is the concentration tensor of phase r and has the following properties,

$$\sum_{r=1}^{N} c_r A_r = I \tag{15}$$

where I is the forth order identity tensor. Combining equations (11–15), the overall electroelastic modulus predicted by the double inclusion model can be expressed as

$$E = E_1 + \sum_{r=2}^{N} c_r (E_r - E_1) A_r \tag{16}$$

where E is the extended electroelastic matrix defined in equation (10) and A is the concentration tensor, which is a function of the eshelby's tensor and the electroelastic properties of the each phase. For the double inclusion model of the three phase composites shown in Figure 1, the concentration tensor is defined as [9]

$$\begin{aligned} A_3^{di} &= I + \Delta S \Phi_2 + S_3 \Phi_3 \\ A_2^{di} &= I + \left[S_2 - \frac{c_3}{c_2} \Delta S \right] \Phi_2 + \frac{c_3}{c_2} \Delta S \Phi_3 \end{aligned} \tag{17}$$

where the S is the eshelby's tensor which is a function of the inclusion geometry as well as the electroelastic properties of the matrix, the explicit expression for a fibrous inclusion can be found elsewhere [7], Φ is the forth order tensor which is a function of the eshelby's tensor and the electroelastic properties of each phase. The expression of Φ is given by the following expression,

$$\Phi_2 = -\left[\Delta S + (S_2 + F_3)\left(S_3 - \frac{c_3}{c_2}\Delta S + F_3\right)^{-1}\left(S_3 - \frac{c_3}{c_2}\Delta S + F_2\right)\right]^{-1}$$
$$\Phi_3 = -\left[(S_2 + F_3) + \Delta S\left(S_3 - \frac{c_3}{c_2}\Delta S + F_2\right)^{-1}\left(S_3 - \frac{c_3}{c_2}\Delta S + F_3\right)\right]^{-1} \quad (18)$$

where the F and ΔS are expressed as

$$F_2 = (E_2 - E_1)^{-1}E_1$$
$$F_3 = (E_3 - E_1)^{-1}E_1 \quad (19)$$
$$\Delta S = S_3 - S_2$$

The geometry of the ASF for the multifunctional composite is shown in Figure 1 with the coordinate system adopted here [10-12]. Because the ASFs are poled along the transverse direction, the piezoelectric coupling e_{32} and e_{33} are along the radial direction of the piezoelectric shell, while e_{31} is along the longitudinal direction. In order to maintain consistency with Eshelby's tensor coordinates system [7, 8], the actual electric field which is applied through the thickness of the piezoelectric layer (along radial direction) must be considered in the global coordinate system. Therefore, to account for the symmetry in the electric field the coupling in the -1 and -2 directions are taken to be equal. Note that the standard convention in composites defines the fiber direction as the -3 direction, therefore in accordance with this convention the piezoelectric axis have been modified from the traditional directions such that the poling axis occurs in both the -1 and -2 directions due to the concentric electrodes.

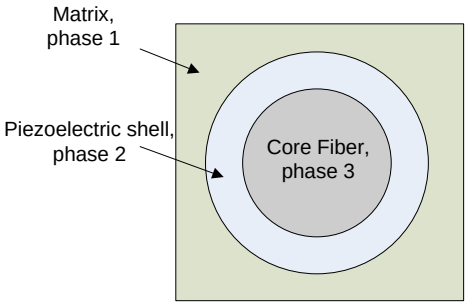

Figure 2. Schematic illustrating of the three phase active composites.

A non-uniform local electric field occurs due to the concentric nature of the electrodes and has been evaluated by Lin and Sodano [10,13]. It has been found that the relation between the local and the global electric field is defined as

$$E_{local} = \frac{-1}{(1/\alpha - 0.5)\ln(1-\alpha)}E \quad (20)$$

where α is the aspect ratio defined as the ratio of piezoelectric shell thickness to the total radius of the ASF, E_{local} is the local electric field added through the thickness of the piezoelectric shell, E is the electric field in the global coordinate system to be consistent with previous modeling analysis [10,13].

3.0 Fabrication and Testing of ASF

The active structural fibers fabricated here have used silicon carbide fibers (Type SCS-6, 140μm diameter, Specialty Materials, Inc. Lowell, MA, USA) as the electrodes and reinforcement, while barium titanate ($BaTiO_3$) powder was used as the piezoceramic constituent. Electrophoretic deposition was used to deposit a film of piezoelectric material with controlled thickness. The process dispersed 3 wt% of $BaTiO_3$ nano-powder ($BaTiO_3$, 99.95%, average particle size: 100nm, cubic phase, Inframat Advanced Materials, Farmington, CT, USA) in 200 mL organic solvent mixture composed of acetone and ethanol (1:1 volume ratio) [14]. The power was deposited on the anode through the action of an electric field. Variation of the field strength and time allowed for control of the deposition thickness. The coated fibers were then sintered in a tube furnace (Thermolyne 79400) at 1200°C for three hours under a nitrogen gas

atmosphere to avoid oxidation of the fiber. It was found that three hours allowed the fibers to reach full density as show in Figure 2. After sintering the fibers, the outer surface of the $BaTiO_3$ layer was coated with silver paint (SPI Supplies, #5002) to form the outer electrode. The silver paint was annealed at 500°C under a nitrogen atmosphere. For bulk $BaTiO_3$, the poling process can be done under DC electric field (2kV/cm) at its curie temperature (120°C) [15]. However due to the fiber geometry shown in Figure 1, the electric field on the inside edge of $BaTiO_3$ is always higher than that of the outside edge, therefore, when poling the fibers 5 times higher field is applied than that required for bulk $BaTiO_3$ in order to produce an adequate field on the outside edge of the $BaTiO_3$. The coated fibers were poled in a silicon oil bath (Sigma-Aldrich, Milwaukee, WI) at 120°C, the electric field used was 10kV/cm with a 60 min holding time. In order to prevent depoling while at its curie temperature, the electric field was maintained until the fibers were cooled to room temperature.

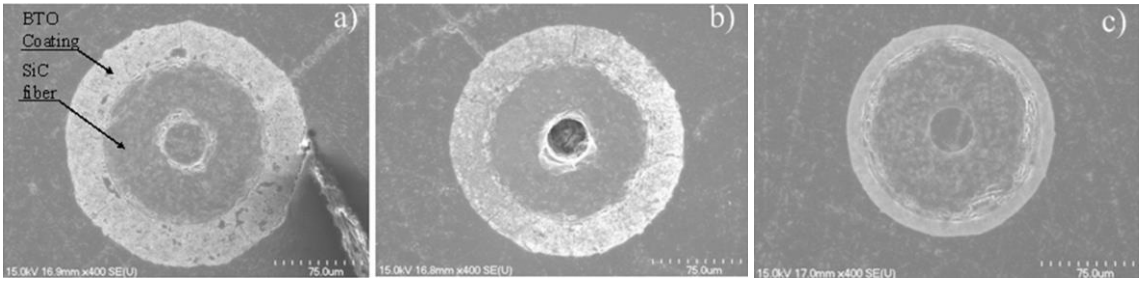

Figure 2: Cross section of the ASF under different sintering conditions, a) Sintered for 1 hours, b) Sintered for 2 hours, c) Sintered for 3 hours.

Once the ASF was fabricated, the single fiber lamina was created by applying an epoxy layer of a specific thickness to achieve a desired volume fraction. Epon 862 resin and 9553 hardener (100:16.9 by weight) were used as the epoxy coating layer, which is cured under room temperature for 24 hours. This epoxy was chosen due to its room temperature curing property which was critical for the coating process here, because the ASF was poled before epoxy coating and if heated above its Curie temperature (120°C) will lose its polarization. The ASF was dip coated with epoxy and carefully smoothed along the entire fiber length to form the concentric cylinder single fiber lamina sample. The fiber volume fraction of each sample was controlled through the number of coatings applied.

In addition to the fabrication of the ASF with a SiC core we have begun to explore the processing of a carbon fiber based active structural fiber. Carbon fiber has a diameter (5mm diameter) better suited for incorporation into composites and can be used with lead based ceramics which have higher electromechanical coupling but react with silicon fibers at high temperature. In order to deposit lead zirconate titanate (PZT) on the carbon fibers cathodic electrolytic deposition is used. The cathodic electrolytic deposition procedure uses a high electric field to deposit ions on the electrode, forming in our case metal oxide deposits on the cathodic substrate. The deposition process is made possible through the generation of a strong base locally at the electrode due to the following reaction

$$2H_2O + 2e^- <==> H_2 + 2OH^-.$$

This hydrolysis reaction results in the accumulation of colloidal particles near the electrode, which are then deposited under the action of the electric field. Following the deposition of the colloidal particles, high temperature processing allows for crystallization of the piezoceramic. The electrolytic deposition process is desirable because it allows uniform coatings to be applied to substrates with complicated surfaces such as carbon fibers, and it can deposit ceramics with control over the stoichiometry, which is important with piezoelectric materials. Additionally, the deposition thickness allows for precise control of the multifunctional materials properties.

The ELD process is carried out in 250 ml stock solutions of solutions of $Pb(NO_3)_2$ (Alfa Aesar), $ZrOCl_2 \cdot 8H_2O$ (Sigma-Aldrich, USA), $TiCl_4$ (Alfa Aesar, USA) and hydrogen peroxide, H_2O_2 (35 wt% in water, Alfa Aesar, USA) in a ratio of 1:0.52:0.48:10 respectively [16]. The net $Pb(NO_3)_2$ concentration was 0.005 M [16]. The $TiCl_4$ was prepared in 25 ml of water before being slowly added into the aqueous solution of $Pb(NO_3)_2$, $ZrOCl_2 \cdot 8H_2O$, and H_2O_2. In order to investigate the influence of a cationic polymer in deposition morphology, different concentrations of poly(diallyl dimethylammonium)chloride (PDDA, 20 wt% in water, Aldrich) were added to some of stock solutions and fully dissolved by stirring vigorously for several minutes. The substrate used was Hexcel HexTow™ IM7 (5000) carbon fibers, a 12 K filament tow. The fibers were cleaned before deposition trials using acetone and ethanol rinses. The electrochemical cell included the carbon fibers (cathode), and two 0.25 mm diameter 99.9% platinum wire electrodes (Aldrich, USA). The power source used was an Agilent E3649A Dual Output DC power supply operating under constant current. All experiments were performed at 2 ◦C [16]. The current density applied through the cell was varied from 5 to 40 mAcm−2. Deposition times ranged from 30 s to 4 min. After deposition, the samples were rinsed with purified water and then were hung to dry in air.

To measure the effective d_{31} value as well as to determine the success of the fabrication process, the longitudinal free strain of several fibers with different aspect ratios were experimentally found by measuring the fiber displacement under field. Both the single fibers and the single fiber lamina were experimentally tested. The testing setup is schematically shown in Figure 3. The samples were first polished on both ends using a diamond lapping film (Allied, diamond lapping film, #50-30076) to form two flat and parallel surfaces. For the lamina samples the polymer coating had to be removed such that electrical connection could be made. This was accomplished by immersing approximately 2 mm of one end of the polished sample in chloroform to remove the epoxy coating and expose the silver paint for electrical connection. Half of the exposed barium titanate coating near the end was then carefully removed, leaving 1 mm of the inner SiC core fiber protruding for electrical connection. The same process was used for the fibers with epoxy; however the chloroform treatment was not necessary. A typical sample after etching is shown in Figure 4. The bare SiC fiber was then passed through a Kapton insulating layer and inserted into section of copper tape that would act as an electrical interconnect. The exterior was then coated with silver paint using the Kapton to separate the two electrodes, as shown in Figure 3. The longitudinal displacement was measured using an AFM (Digital Instruments/Veeco MultiMode AFM). The excitation signal used to actuate the fiber was a sine wave (V_{pp} = 10 V, f = 200 mHz) generated by a function generator (Agilent, 33220A).

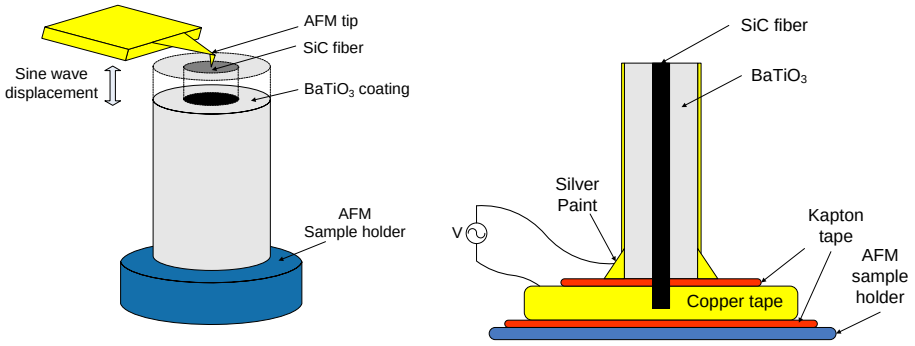

Figure 3: Schematic of the experiment setup for the effective piezoelectric coupling d_{31}.

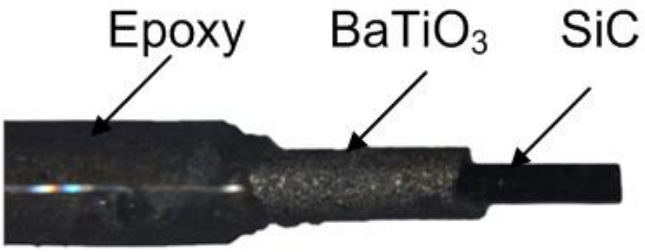

Figure 4: Image of the single active structural fiber lamina coating process, resulting is several concentric phases.

4.0 Results and Discussion

According to Equation (7), the measured displacement was converted to effective d_{31} coupling for the piezoelectric fiber. The coupling was divided by the d_{31} value of the bulk materials and compared with the results from the FE and micromechanics models presented by Lin and Sodano [13]. The experimental error has been calculated through an analysis of the error in each measurement and the consideration of it propagation to the measured coupling. Figure 5 presents the results of our testing compared to those calculated through the micromechanics model presented in Section 2 and a FE model developed using ABAQUS (detailed in Ref [13]) with respect to the fiber aspect ratio. It can be seen in the figure that excellent agreement between the FEA, micromechanics model and experiments is achieved. As expected, the effective d_{31} increased with aspect ratio, however, the maximum value is obtained when the aspect ratio is approximately 0.8, which corresponds to the point at which the surface area of the inner wall becomes much less than the outer wall resulting in a break down of the thin wall approximation. Our experimental testing could only achieve aspect ratios up to 0.67 because the high aspect ratio leads to very high electric field on the inner wall making poling difficult.

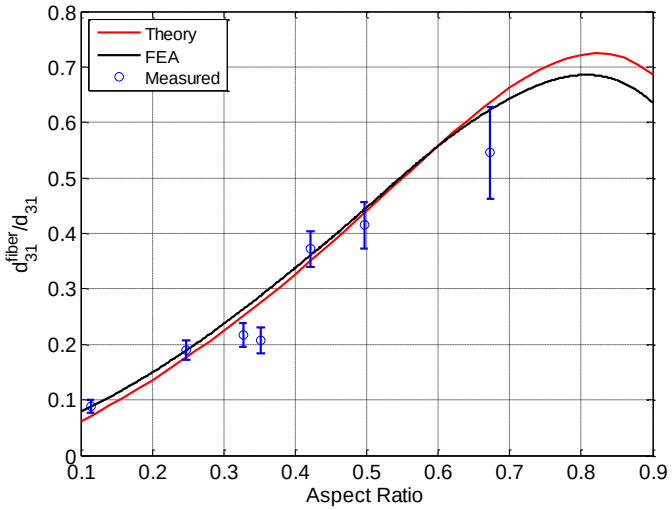

Figure 5: Comparison of FEA and measured coupling coefficients for active fibers with respect to the aspect ratio (t/r_0) of the piezoelectric material.

Using a similar process to the single fiber specimens the electromechanical coupling of the single active structural fiber embedded in an epoxy layer was measured and is shown in Figure 6 along with the predictions from the double inclusion model. There is excellent agreement between the model and experimental measurements for samples with aspect ratio of 0.21 and 0.42 for the entire fiber volume fraction range. Although the measured d_{31} values for fibers with an aspect ratio of 0.61 follow the same trend as that of the model, the measurements fall below the estimated coupling for the entire fiber volume

fraction range. The results are consistent with the findings of the single fiber data plotted in Figure 5. A possible reason for the slightly lower than expected coupling is due to the significant difference between the inner and outer electrode surface area which results in a higher electric field at the inner wall and a lower electric field at the outer wall. While this varying field is captured by the model, during fabrication it is difficult to achieve the required poling field on the outer wall leading to only partial polarization and lower bulk coupling. This effect is accounted for with a higher than required poling voltage, however we believe this result still occurs for high aspect ratios due to breakdown of the inner wall before full polarization.

The results presented in Figures 5 and 6 demonstrate the accuracy of our theoretical models and the validity of the experimental techniques developed here. These results also demonstrate that the active structural fiber proposed could be used to provide composite materials with significant electromechanical coupling, approaching than 60% of the active constituent. The use of this new piezoelectric fiber composite would allow multifunctional materials to be designed that offer load bearing, and sensing/actuation properties for a wide variety of applications including structural sensing, actuation, self-monitoring, power harvesting, or shape control through anisotropic actuation

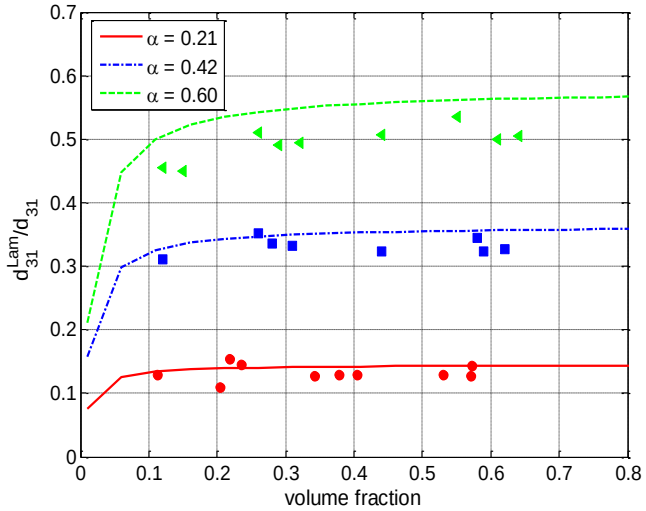

Figure 6: Comparison of FEA and measured coupling for active structural lamina for three different aspect ratio (t/r_0) piezoelectric coating with respect to the volume fraction of the ASF.

The high dielectric properties of the barium titanate shell applied to the SiC core fiber make the active structural fiber an outstanding candidate for converting and storing ambient mechanical energy into electrical energy to power other electric devices in a system. The capacitance of four aspect ratio multifunctional fibers as a function of electrical field frequency (100-10000 Hz) is measured using a HP LCR meter (HP 4284A). The multifunctional fiber was attached onto two silver paint coated carbon tape electrodes, one connected to the SiC as the inner electrode and one connected to the outer surface of the multifunctional fiber as the other electrode. The breakdown voltage testing was performed according to the ASTM standard D149. Two 6.35 mm cylindrical brass rods with one end rounded to 0.76 mm were used as the probes. Due to the unique geometry of the multifunctional fiber, the breakdown voltage testing was performed on the same sample set up as that for the capacitance testing. However was performed in a silicone oil bath to reduce environmental effects. Four different aspect ratio sets (aspect ratios α of 0.15, 0.23, 0.42 and 0.54) and five samples for each aspect ratio were fabricated and tested. Figure 7 shows the side and cross section view of typical fibers tested.

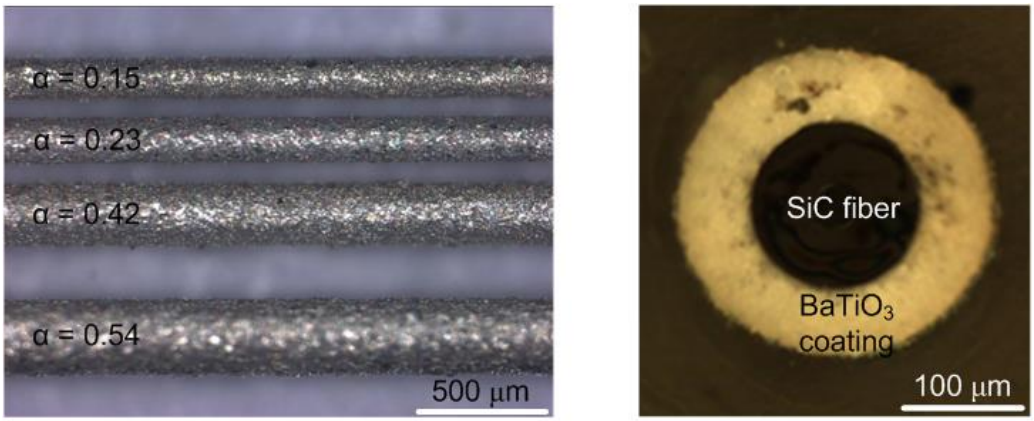

Figure 7: Side and cross section view of a typical samples, (a) side view of four different aspect ratio multifunctional fibers, (b) cross section view of $\alpha = 0.42$ multifunctional fiber.

The most important factor in the design of a structural capacitor is the energy density, which is defined as the ratio of maximum stored energy in the capacitor and total volume of the capacitor and is expressed as,

$$E = \frac{1}{2}CV^2 \tag{21}$$

where E is stored energy, C is the capacitance of a capacitor, V is the voltage applied to the capacitor. Structural capacitors offer the opportunity for significant volume and mass reduction compared with material system using separate structural and energy storage components. The dielectric strengths for low aspect ratio fibers (0.15 and 0.23) are 6.5722 and 7.4003 MV/m, while high aspect ratio fibers (0.42 and 0.54) show a reduced dielectric strength of 3.2010 and 2.5689 MV/m, respectively. The non-uniform electric field density on the inner and outer surface of the BaTiO3 coating causes the reduced dielectric strength with increased aspect ratio. The smaller inner electrode has a much higher electric field per unit area at breakdown than the outer electrode, which suggests the breakdown occurs at the inner wall then gradually spreads to the outer layer until the outer surface of material breaks down and thus the entire multifunctional fiber fails. The energy density for each tested aspect ratio is shown in Figure 8. The highest energy density measured is 0.117 MJ/m^3 for an aspect ratio of 0.23. For lower aspect ratio fibers the capacitance is higher than that of the 0.23 aspect ratio fiber, however, the breakdown voltage is lower due to its thinner dielectric material. Also the volume fraction of the $BaTiO_3$ is lower for lower aspect ratio fibers, which decreases energy density. Compared with structural capacitor developed based on glass or polymer fiber composites, the energy density of the multifunctional fiber with 0.23 aspect ratio is about two orders of magnitude higher. With such a high energy density, structures composed of the capacitive fiber will have a strong potential to provide structural composites with excellent embedded energy storage.

In addition to the testing of SiC fiber samples, experiments have been performed to demonstrate that the electrolytic deposition process can be used to individually coat carbon fibers while in a tow. This process used a water solution of $Pb(NO_3)_2 : ZrOCl_2 : TiCl_4 : H_2O_2$ mixed in a ratio of 1 : 0.52 : 0.48 : 2.4 with a $Pb(NO_3)_2$ concentration of 0.005 M. The water bath was held at 2°C and the carbon fiber was used as the cathode and two platinum wires as the anode. A galvanostat (Princton Applied Research, Model 273) was used to maintain a current density of 25 mA/cm^2 during the deposition process. The deposition time was 5 minutes followed by annealing at 300°C for 5 minutes then calcination at 600°C for 1 hour. The microstructure of the coating was studied using a field emission scanning electron microscopy

(Hitachi, FESEM-4700) and is shown in Figure 9. From this figure, it can be seen that the deposition process is capable of uniformly coating individual fibers with lead ziconate titanate (PZT); however, the coating exhibits some cracking. This phase of the research will investigate two methods to generate crack free films, namely the use of hydrogen peroxide (H_2O_2) and cationic polyelectrolytes (water soluble polymers carrying ionic charge along the polymer chain). These two methods will be evaluated to enhance the microstructure of the films during this phase of the research. Figure 9 shows preliminary results from the use of a PVA binder and shows very good coating morphology with no cracking.

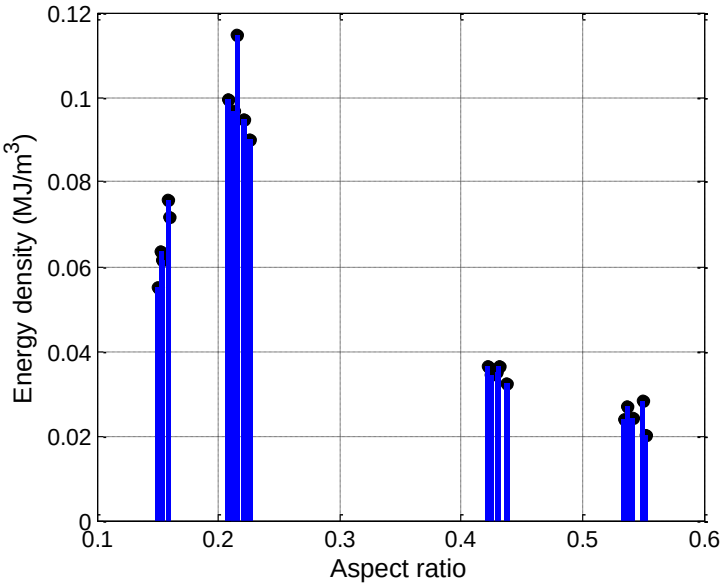

Figure 8: Energy density for each aspect ratios samples.

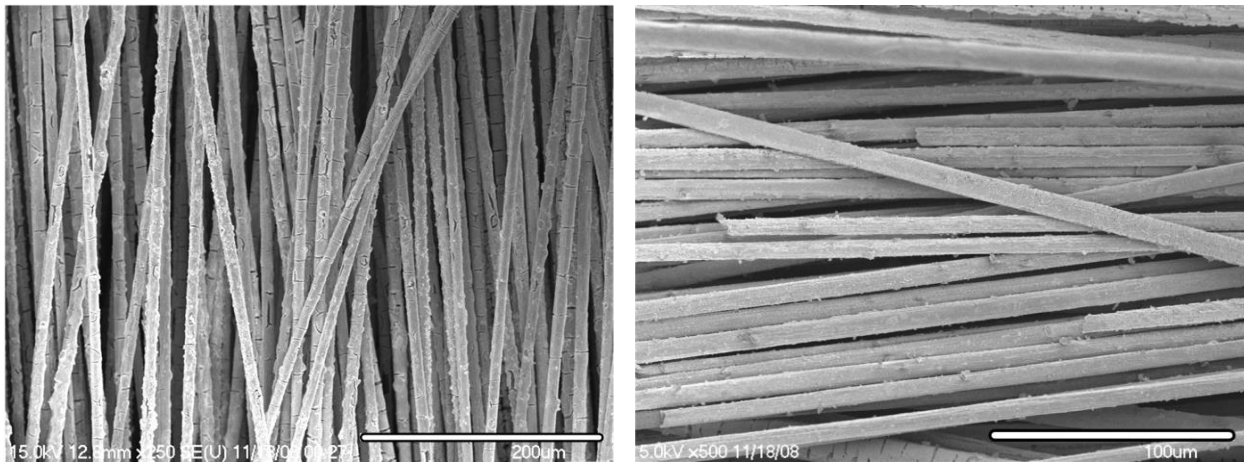

Figure 9: PZT deposited on a 3k tow of carbon fiber using cathodic electrolytic deposition (left), and deposited using 2g/L of PVA binder (right).

In addition to the use of electrolytic deposition approaches for the coating of carbon fibers with piezoceramic materials a hydrothermal process has been developed to coat carbon fiber with Barium titanate. The fabrication of $Ba_xSr_{1-x}TiO_3$ (BST) films on carbon fiber is accomplished by a two-step hydrothermal reaction. First, a TiO_2 nanowire array is grow onto carbon fiber filament (IM8, Hexcel) using a similar method as mentioned elsewhere [17], leaving a 1cm long section uncoated such that the fiber can be accessed and used for testing. After the TiO_2 nanowires were grown on the carbon fiber, it

was then transferred to $Ba_xSr_{1-x}TiO_3$ by hydrothermal reaction with aqueous solution containing $Ba(OH)_2 \cdot 8H_2O$ and $Sr(OH)_2 \cdot 8H_2O$. In order to study the influence of the ratio of barium and strontium on the energy density of the film, BST films with 7 different ratios of Ba:Sr were fabricated. A 10 nm gold coating was sputtered (Pelco SC-7) on the BST film to serve as the other electrode for experimental testing. Finally, the BST coated carbon fiber is mounted onto a microscope slide with two drops silver paint on the exposed carbon fiber and gold-coated section of BST such that the dielectric and energy storage properties could be identified.

Typical SEM images of carbon fibers coated with a BST film are shown in Figure 10. After transferring the TiO_2 to barium strontium titanate, the film's surface becomes rough although the core of the film is dense with no voids or cracks as shown in Figure 2b. This growth of crystals on the surface during the transformation from TiO_2 to $Ba_xSr_{1-x}TiO_3$ has been found in a similar synthesis process of BST particles [17]. In order to confirm the TiO_2 nanowires have been fully transformed to BST, the crystal structure before and after transfer to barium titanate or barium strontium titanate is characterized by X-ray diffraction (XRD). The XRD trace is shown in Figure 11 and demonstrates the peak shift with an increased strontium concentration. The upward shift occurs because the lattice spacing of strontium titanate (3.905Å) is smaller than that of barium titanate (4.038Å), which according to Bragg's law produces diffraction at higher angles with increasing strontium [18]. The XRD spectrums of transferred BST fibers do not contain any peaks from TiO_2, thus indicating the films are fully transferred, which is critical for high energy storage density since TiO_2 has a low dielectric permittivity.

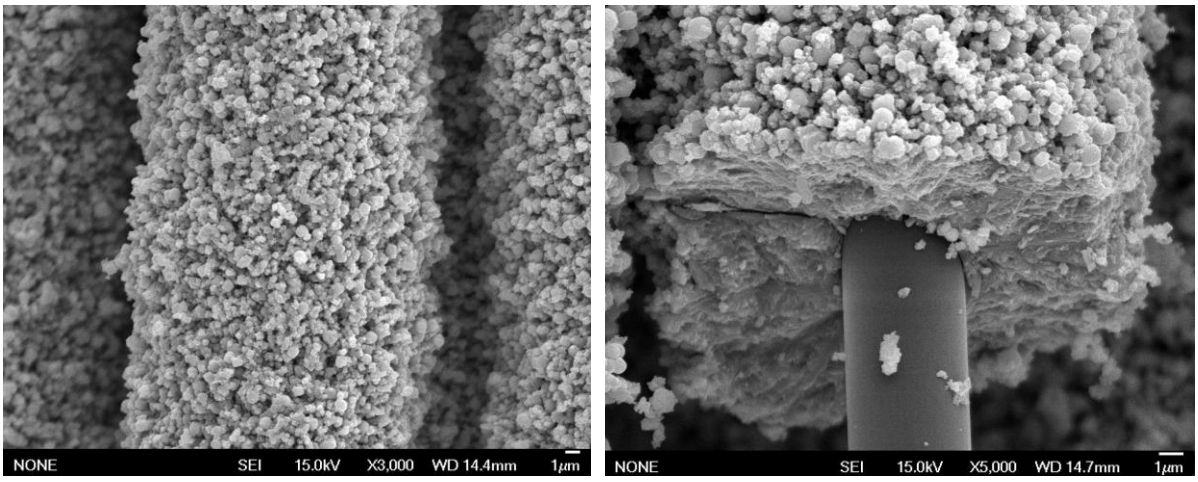

(a) (b)

Figure 10. SEM images of multifunctional fiber, (a) BST coating on carbon fiber and (b) cross section of BST coated carbon fiber showing high density core.

An LCR meter (Agilent E4980A) was used to measure the capacitance of individual multifunctional fibers with various BST compositions. After the dielectric of each sample was measured, the dielectric strength of the capacitor was measured in accordance with ASTM standard D149-97a. As can be seen in Figure 5, the dielectric constant of BST ranges from 578 to 2854, and peaks at a composition of $Ba_{0.71}Sr_{0.29}TiO_3$ since this composition has its T_c is closest to ambient. However, the dielectric constant is lower than other previously published data. Several possible reasons for this comparatively low dielectric constant exist, such as the roughness of the BST surface as indicated in Figure 2, and the possibility of a small portion of TiO_2 impurities which may significantly reduce the dielectric. However, the dielectric constant of certain compositions such as $Ba_{0.6}Sr_{0.4}TiO_3$ and $Ba_{0.71}Sr_{0.29}TiO_3$ are more than two times

higher than that of BTO, leading to the potential for the development of multifunctional structures with significantly enhanced energy storage capacity.

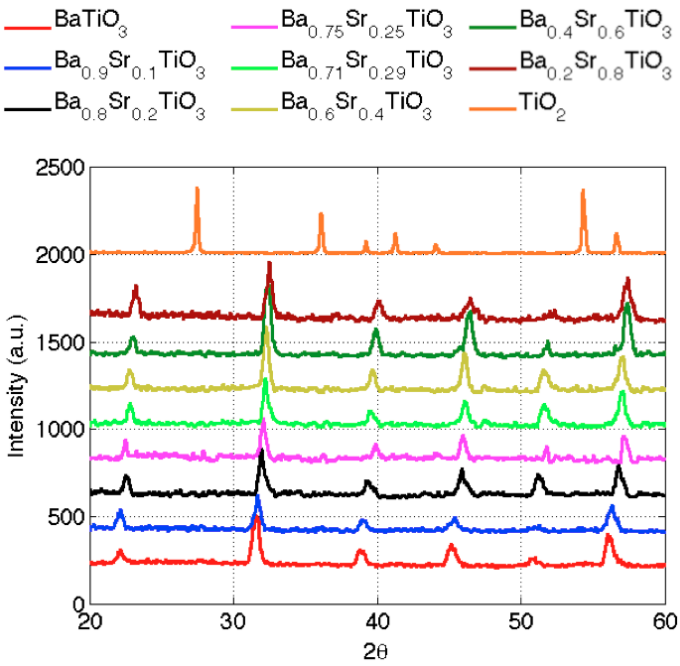

Figure 11. XRD scan of various BST films on carbon fibers.

Following the measurement of the dielectric constant for each sample, dielectric strength testing was performed to characterize the energy storage capacity of the fiber. The dielectric strength is calculated by dividing the breakdown voltage by the thickness of BST coating and is shown in Figure 6. The dielectric strength shows a maximum value just before the ceramic transitions form tetragonal to cubic at $Ba_{0.71}Sr_{0.29}TiO_3$. This trend can be explained by the phase transformation between cubic and tetragonal crystal structures. It has been shown that the breakdown strength of BTO also peaks around the T_c due to this phase transition [19].

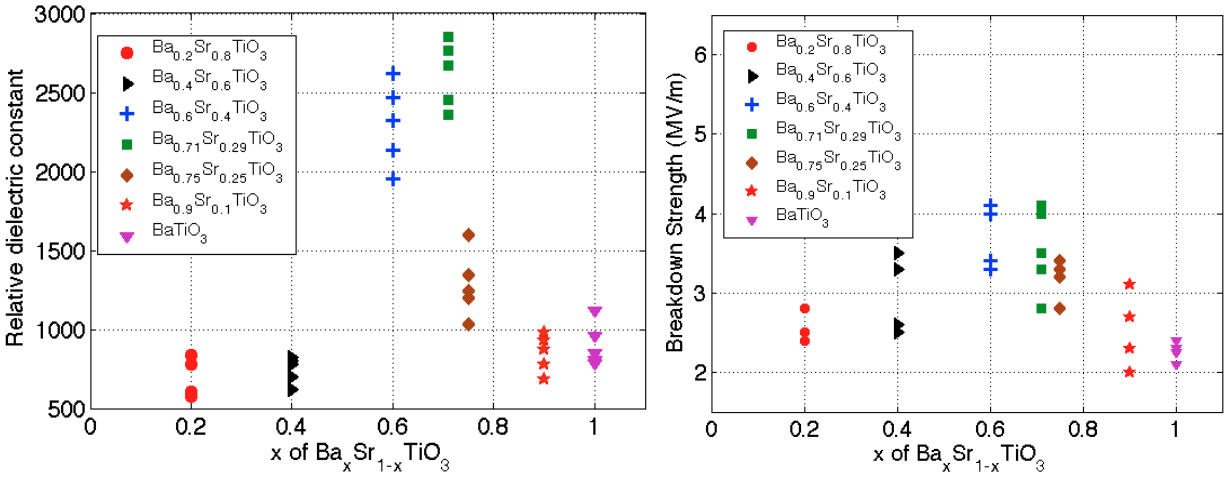

Figure 12. Relative dielectric constant of BST films as a function of BST composition (left) and breakdown strength of BST films as a function of BST composition (right).

From the dielectric constant and the breakdown strength the energy density is defined as the ratio of maximum stored dielectric energy to the total volume can be calculated for a concentric capacitor. All tested samples have similar geometry and the dielectric constant and breakdown strength show a similar trend; therefore, the energy density for each fiber should follow. The energy densities for each fiber are calculated and presented in Figure 13. The BST composition with the highest energy density occurs with $Ba_{0.71}Sr_{0.29}TiO_3$ or when the T_c is at ambient temperature, with an average energy density of 0.12J/cc. Compared to other structural capacitors appearing in the literature, the energy density is comparable or higher depending on the dielectric medium used. The novel multifunctional fiber utilizes the carbon fiber as both the inner electrode and the load-bearing component, allowing easy integration into existing high performance carbon fiber composites. The structural capacitor based on SiC fiber is limited to single fiber fabrication and is challenging to scale to a laminate level fabrication. Since the aspect ratio was not considered here and was shown to be a major factor in the performance of the SiC fibers, the energy density of the carbon based structural capacitor is more than 5 times higher that of the SiC based capacitor at the same aspect ratio.[22] It is expected that using thinner BST coatings could significantly increase the energy density of this carbon fiber based structural capacitor by reducing the electric field density at the inner electrode. This could be accomplished through a modification of our synthesis methods.

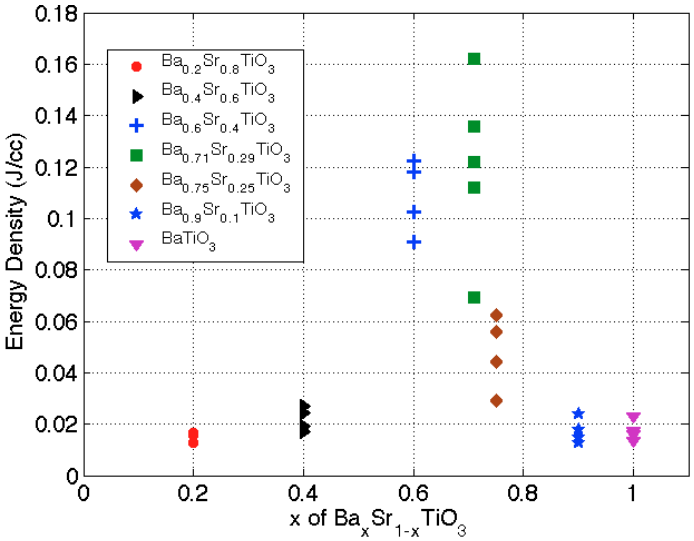

Figure 13. Energy density of multifunctional fibers as a function of BST composition.

Conclusions

This research effort has developed a novel multifunctional system based on the combination of piezoelectric materials and fiber reinforced composites. The work has lead to the development of multi-inclusion models to predict the constitutive properties of the composites with three phases and synthesis approaches have been developed for both SiC and carbon fiber. Experiments and finite element studies have been used to validate the models and demonstrated excellent agreement. It has been demonstrated that a structural composite utilizing a low volume fraction (~30%) could retain nearly 60% of the coupling of the piezoelectric phase. Depending on the piezoceramic used this result would lead to rigid composites that had bulk coupling greater than many monolithic materials. Furthermore, the work has developed new synthesis approaches for the coating of small diameter (5μm) carbon fiber and the energy storage capabilities of such composites.

References

[1] Sodano, H.A., Park, G. and Inman, D.J., "Multiple Sensors and Actuators for Vibration Suppression of an Inflated Torus, *AIAA Journal of Spacecraft and Rockets*, 2005; 42(2): 370-373.

[2] Sodano, H.A., Park, G. and Inman, D.J., "An Investigation into the Performance of Macro-Fiber Composites for Sensing and Structural Vibration Applications," *Mechanical Systems and Signal Processing*, 2003; 18(3): 683-697.
[3] Sebald, G., Qiu, J., Guyomar, D. and Hoshi, D., "Modeling and Characterization of Piezoelectric Fiber with Metal Core," *Japanese Society of Applied Physics*, 2005; 44(8): 6156-6136.
[4] Takagi, K., Sato, H. and Saigo, M., "Vibration control of a smart structure embedded with metal-core piezoelectric fibers," *Advanced Composite Material*, 2006; 15(4):403-417.
[5] Sato, H., "Development of multifunctional wire that combineds shape-memory alloy to piezoelectric material," *Proceedings of SPIE 15th Annual International Symposium on Smart Structure/NDE*, vol. 6929, San Diego, CA, 2008
[6] Hori, M. and Nemat-Nasser. S., "Double-inclusion model and overall moduli of multi-phase composites," *Mechanics of Materials*, Vol. 14, 1993, pp.189-206.
[7] Dunn, M. L., Taya, M., "Micromechanics predictions of the effective electroelastic moduli of piezoelectric composites," *International Journal of Solids Structures*, Vol. 30, 1993, pp. 161-175.
[8] Odegard, G. M., "Constitutive modeling of piezoelectric polymer composites," *Acta Materialia*, Vol. 52, 2004, 5315-5330
[9] Dunn, M. L., Ledbetter, H., "Elastic moduli of composites reinforced by multiphase particles," *Journal of Applied Mechanics*, Vol. 62, 1995, pp. 1023-1028.
[10] Lin, Y. and Sodano, H.A., 2008, "Concept and Model of a Piezoelectric Structural Fiber for Multifunctional Composites," *Composites Science and Technology*, **68** (7-8):1911-1918.
[11] Lin, Y. and Sodano, H.A., 2009, "Fabrication and Electromechanical Characterization of a Piezoelectric Structural Fiber for Multifunctional Composites," *Advanced Functional Materials*, **19**: 1-7.
[12] Lin, Y. and Sodano, H.A., 2009, "Electromechanical Characterization of a Multifunctional Active Structural Fiber Lamina," *Composites Science and Technology*, **69**: 1825–1830.
[13] Lin, Y. and Sodano, H.A., 2009, "Double Inclusion Model for Multifunctional Piezoelectric Composites," Proceedings of the 50th AIAA/ASME/ASCE/AHS/ASC Structures, Structural Dynamics and Materials Conference (SDM), May 4-7th, Palm Springs, CA.
[14] R.F. Louh and Y.H. Hsu, Fabrication of barium titanate ferroelectric layers by electrophoretic deposition technique, *Mater. Chem. Phys.* **79** (2003), pp. 226–229.
[15] Lu HA, Wills LA, Wessels BW., 1994, Electrical properties and poling of BaTiO3 thin films. Appl. Phys. Lett., 64:2973.
[16] Zhitomirsky I, Gal-Or L and Kohn A, 1997, Electrolytic PZT Films, *J. Mater. Sci.* **32:**803–7
[17] Wang, Y., XU H., Wnag, X., Zhang, X., Jia, H., Zhang L. and Qiu J. 2006. A general approach to porous crystal TiO_2, $SrTiO_3$ and $BaTiO_3$ Spheres, *The Journal of Physical Chemistry B*, **110**: 13835-13840.
[18] Fu, C., Yang, C., Chen, H., Wang Y. and Hu L. 2005. Microstructure and dielectric properties of $Ba_xSr_{1-x}TiO_3$ ceramics, *Materials Science and Engineering B*, **119**: 185-188.
[19] Fang P.H. and Brower W.S. 1959. Temperature dependence of the breakdown field of barium titanate, *Physical Review*, **113**: 455-457.

Publications Resulting from this Work

23. Lin, Y., Zhi, Z. and Sodano, 2012, "Barium Titanate and Barium Strontium Titanate Coated Carbon Fibers for Multifunctional Structural Capacitors," *Journal of Composite Materials*, In Review.

24. Zhou, Z., Lin, Y. and Sodano, H.A., Synthesis and Characterization of Textured BaTiO3 Thin Films, 36th International Conference and Expo on Advanced Ceramics and Composites, January 22 – 27, 2012, Daytona Beach, FL.

25. Sodano, H.A., 2011, "Nanowire Interfaces for Simultaneously Increased Strength and Functionality,

Composites at Lake Louise Conference, October 30th – November 4th, Alberta, Canada (Invited Speaker).

26. Sodano, H.A., 2011, "Multifunctional Materials and Nanocomposites for Energy Storage," Nanotechnology for Defense Conference (NT4D), October 24 – 27, Bellevue, WA (Invited Speaker).

27. Sodano, H.A., 2011, "Multifunctional Solutions for Piezoelectric Energy Harvesting," International Symposium on Green Manufacturing and Applications (ISGMA 2011), October 6 – 7, Seoul National University, Seoul, Korea (Keynote Speaker).

28. Lin, Y. and Sodano, H.A., 2010, "Enhanced piezoelectric properties of lead zirconate titanate sol-gel derived ceramics using single crystal $PbZr_{0.52}Ti_{0.48}O_3$ cubes," *Journal of Applied Physics*, 108, 064108.

29. Lin, Y., Zhou, Z. and Sodano, H.A., 2011, "Multifunctional Structural Capacitors Consisting of Barium Titanate and Barium Strontium Titanate Coated Carbon Fibers, 18th International Conference on Composite Materials, August 21-26, Jeju Island, South Korea.

30. Lin, Y. and Sodano H.A. 2011 "Multifunctional Structural Capacitors Consisting of Barium Strontium Titanate Coated SiC Fibers," Electronic Materials and Applications 2011, Jan. 19th–21st Orlando, FL (Invited).

31. Lin, Y., Shaffer, J.W. and Sodano, H.A., 2010, Electrolytic Deposition of PZT on Carbon Fibers for Multifunctional Composites, *Smart Materials and Structures*, **19**: 124004 (Invited paper).

32. Lin, Y. and Sodano, H.A., 2010, "Double Inclusion Model for Multiphase Piezoelectric Composites," *Smart Materials and Structures*, **19**: 035003.

33. Lin, Y. and Sodano H.A., 2009, "Characterization of Multifunctional Structural Capacitors for Embedded Energy Storage," *Journal of Applied Physics*, **106**: 114108.

34. Lin, Y. and Sodano, H.A., 2009, "Electromechanical Characterization of a Multifunctional Active Structural Fiber Lamina," *Composites Science and Technology*, **69**: 1825–1830.

35. Lin, Y. and Sodano, H.A., 2009, "Fabrication and Electromechanical Characterization of a Piezoelectric Structural Fiber for Multifunctional Composites," *Advanced Functional Materials*, **19**: 1-7.

36. Lin, Y. and Sodano, H.A., 2008, "Concept and Model of a Piezoelectric Structural Fiber for Multifunctional Composites," *Composites Science and Technology*, **68** (7-8):1911-1918.

37. Lin, Y. and Sodano, H.A., 2009, "Double Inclusion Model for Multiphase Piezoelectric Composites," *Smart Materials and Structures*, In Review.

38. Shaffer, J.W., Lin, Y. and Sodano, H.A., 2009, Electrolytic Deposition of PZT on Carbon Fibers for Multifunctional Composites, Proceeding of the 15th International Conference on Adaptive Structures and Technologies (ICAST), October 20th – 22nd, Hong Kong, China.

39. Lin, Y. and Sodano H.A., 2009, "Characterization of Multifunctional Structural Capacitors for Embedded Energy Storage," ASME's 2nd Annual Conference on Smart Materials, Adaptive Structures

and Intelligent Systems, September 21st-23rd Oxnard, CA.

40. Lin, Y. and Sodano, H.A., 2009, "Double Inclusion Model for Multifunctional Piezoelectric Composites," Proceedings of the 50th AIAA/ASME/ASCE/AHS/ASC Structures, Structural Dynamics and Materials Conference (SDM), May 4-7th, Palm Springs, CA.

41. Lin, Y. and Sodano, H.A., 2009, Electromechanical Characterization of Single Active Structural Fiber for Multifunctional Composites, Proceeding of the 15th International Conference on Adaptive Structures and Technologies (ICAST), October 20th – 22nd, Hong Kong, China.

42. Lin, Y. and Sodano, H.A., 2009, "Electromechanical Characterization of a Single Fiber Lamina for Multifunctional Composites," SPIE's 16th annual International Symposium on Smart Structures and Materials, March 8th-12th, San Diego, CA.

43. Lin, Y. and Sodano, H.A., 2008, "Fabrication and Electromechanical Characterization of a Piezoelectric Structural Fiber for Multifunctional Composites," 2008 SAMPE Fall Technical Conference, Sept. 8-11th, Memphis, TN. ***(Awarded Best Paper)***

44. Lin, Y. and Sodano, H.A., 2008, "Concept and Model of a Piezoelectric Structural Fiber for Multifunctional Composites," SPIE's 15th annual International Symposium on Smart Structures and Materials, March 9th-13th, San Diego, CA.